The Astrophysical Journal, 868:111 (8pp), 2018 December 1 https://doi.org/10.3847/1538-4357/aae923

The Evolution of the Warm Absorber Reveals a Shocked Outflow in the Narrow Line Seyfert 1 Galaxy IRAS 17020+4544

Mario Sanfrutos[1], Anna Lia Longinotti[2], Yair Krongold[1], Matteo Guainazzi[3], and Francesca Panessa[4]
[1] Instituto de Astronomía, Universidad Nacional Autónoma de México, A. P. 70264, 04510 CDMX, México; sanfrutoscm@astro.unam.mx
[2] CONACYT-Instituto Nacional de Astrofísica, Óptica y Electrónica, Luis E. Erro 1, Tonantzintla, Puebla, C.P. 72840, México
[3] ESTEC/ESA, Keplerlaan 1, 2201AZ Nordwijk, The Netherlands
[4] INAF/Istituto di Astrofisica e Planetologia Spaziali di Roma, via del Fosso del Cavaliere 100, I-00133, Roma, Italy
Received 2018 June 15; revised 2018 September 18; accepted 2018 October 15; published 2018 November 29

Abstract

We present the analysis of grating spectra of the Narrow Line Seyfert 1 Galaxy IRAS 17020+4544 observed by *XMM-Newton* in 2004 and 2014. In a previous work on these data, we reported the discovery of a multicomponent ultra-fast outflow that is capable of producing feedback in the host galaxy. We also reported the presence of a slow, multiphase warm absorber (WA). In this follow-up paper, we confirm that this low-velocity absorber can be modeled by four layers of ionized gas. When crossing our line of sight, this gas presents peculiar changes along the 10 yr timescale elapsed between the two observations obtained by *XMM-Newton*. While two of such components are almost stationary, the other two are found inflowing and outflowing with significant variations in velocity and ionization between 2004 and 2014. The luminosity and spectral shape of the central source remain practically unvaried. We propose that the presence of the fast wind and of the variable WA can be interpreted in the framework of a "shocked outflow," where the peculiar variability pattern of the low-velocity components might arise from instabilities in the shocked gas.

Key words: galaxies: active – galaxies: Seyfert – X-rays: galaxies

1. Introduction

The warm absorber (WA) was first proposed by Halpern (1984) as a cloud or shell of photoionized material in active galactic nuclei (AGNs), in order to explain the X-ray spectrum of the QSO MR 2251–178, whose main signature was first interpreted to be the K-edge of O VII at 739 eV.

In early samples of Seyfert Galaxies observed with the CCD detectors on board the Advanced Satellite for Cosmology and Astrophysics (ASCA), at least half of the type 1 AGNs show high-ionization oxygen K-shell absorption edges (the already mentioned O VII, and O VIII at 0.87 keV) typical of the WA (Reynolds 1997; George et al. 1998); today we know that absorption is produced by a realm of atomic transitions that result in a series of absorption lines from ionized elements (see, e.g., Kaastra et al. 2000; Kaspi et al. 2000, 2002; Blustin et al. 2003; Krongold et al. 2003, 2005a, 2005b; Laha et al. 2014). Most features revealing the presence of WAs are imprinted on the soft X-ray spectra of AGNs. Ionized gas along the line of sight of Seyfert Galaxies has provided an excellent diagnostic for the properties and conditions of photoionized material intrinsic to AGNs. The origin of the WA has sometimes been related to an outflow arising from the dusty torus (Krolik & Kriss 2001; Blustin et al. 2005; Miniutti et al. 2014). Results by Kaastra et al. (2012) on *XMM-Newton* observations of Mrk 509 point to an origin of the WA components in the narrow line region (NLR) or torus region of this object. In other cases, the response of the ionization state of the gas and, in general, variability of the absorber parameters have suggested that the inner accretion disk can be identified as the outflow launching region (Krongold et al. 2007; Longinotti et al. 2013; Kaastra et al. 2014). Mixed situations where different components of the wind are launched in distinct regions of the AGNs show that we are still far from reaching a homogenous picture to explain the absorber phenomenology. For instance, this was the case reported by Sanfrutos et al. (2016) in ESO 323-G77, where we found one variable, "disk-like" WA component from the dust-free broad line region (BLR), and one persistent, "torus-like" component from the dusty, clumpy torus, showing absorption variability at both short and long timescales.

The velocity to which the ionized gas is accelerated is used to separate the standard, "slow" WAs with $v_{out} \lesssim 10^4$ km s^{-1} from the more recently discovered ultra-fast outflows (UFOs), which reach outflow velocities of 0.1–0.3 c (Tombesi et al. 2012; Gofford et al. 2013) and which seem to provide a key ingredient for triggering energy-driven outflows at large scale (Feruglio et al. 2015; Tombesi et al. 2015).

There have been attempts to explore the relation between WAs and UFOs (Tombesi et al. 2013; Laha et al. 2016). Nevertheless, the paucity of sources where these two components of the inner X-ray outflow are observed at the same time with comparable detail and signal-to-noise does not allow firm conclusions to be reached.

IRAS 17020+4544 is a narrow line Seyfert 1 (NLS1) galaxy (Moran et al. 1996; Wisotzki & Bade 1997) at redshift $z = 0.0604$ (de Grijp et al. 1992), with a central supermassive black hole (SMBH) of mass $M_{BH} \sim 5.9 \times 10^6 M_\odot$ (Wang & Lu 2001). Its X-ray luminosity is $\sim 1.5 \times 10^{44}$ erg s^{-1}, from which a bolometric luminosity of $\sim 5.2 \times 10^{44}$ erg s^{-1} is estimated by assuming a correction $k = 10$ (Marconi et al. 2004).

The presence of a dusty WA in this galaxy was first suggested by Leighly et al. (1997) based on data obtained by the *ASCA* satellite and later confirmed by Komossa & Bade (1998) using data from the *ROSAT* mission. The first spectroscopic study of IRAS 17020+4544 with modern X-ray observatories is reported by Longinotti et al. (2015; hereafter L15), who discovered a multicomponent UFO via detection of absorption lines in the *XMM-Newton* grating spectrum. The ionized gas was found to be outflowing at

Table 1
Parameters of the Four WA Components and Four UFOs Detected in the Merged RGS Data Representative of the 2014 Left) and 2004 Right) Spectra

Component	2014					2004				
	log U	log N_H[a]	v_{turb}[b]	v[c]	ΔC	log U	log N_H[a]	v_{turb}[b]	v[c]	ΔC
WA 1 rest)	$-1.88^{+0.03}_{-0.02}$	$21.09^{+0.01}_{-0.01}$	160 ± 30	320 ± 70	530	$-2.10^{+0.07}_{-0.06}$	$21.01^{+0.03}_{-0.11}$	170 ± 60	380 ± 160	100
WA 2 rest)	$-0.57^{+0.05}_{-0.04}$	$21.12^{+0.03}_{-0.04}$	<40	430 ± 90	120	$-0.57^{+0.08}_{-0.11}$	$21.25^{+0.11}_{-0.20}$	<50	490 ± 110	61
WA 3 outflow)	2.47 ± 0.02	20.93 ± 0.01	<40	2300 ± 200	90	$-2.81^{+0.07}_{-0.19}$	$20.88^{+0.03}_{-0.03}$	<60	4000 ± 200	34
WA 4 inflow)	$0.35^{+0.11}_{-0.16}$	$20.84^{+0.16}_{-0.14}$	100 ± 60	1750 ± 250	24	$-1.3^{+0.3}_{-0.4}$	$20.6^{+0.2}_{-0.4}$	110 ± 70	2900 ± 200	14
UFO 1	$-2.47^{+0.15}_{-0.19}$	$20.10^{+0.06}_{-0.09}$	50[f.]	26900 ± 200	27	$-2.2^{+0.3}_{-0.2}$	20.4 ± 0.2	50[f.]	28500 ± 1000	9
UFO 2	$2.63^{+0.04}_{-0.13}$	23.70 ± 0.15	50[f.]	”	7					
UFO 3	$-0.35^{+0.12}_{-0.19}$	$20.4^{+0.2}_{-0.4}$	50[f.]	24100 ± 100	5	$-0.30^{+0.05}_{-0.07}$	$21.27^{+0.15}_{-0.19}$	50[f.]	23900 ± 100	36
UFO 4	$-1.22^{+0.10}_{-0.05}$	$20.85^{+0.03}_{-0.06}$	50[f.]	”	4					

Notes. Fit to 2014 data left): C dof = 3045 2738, $\Gamma = 2.99^{+0.04}_{-0.01}$; Fit to 2004 data right): C dof = 2848 2748, $\Gamma = 2.99^{+0.17}_{-0.07}$.
[a] N_H in cm 2.
[b] Microturbulent velocity of the gas in km s 1.
[c] Velocity component along the line of sight in km s 1. Negative positive values, respectively, refer to inflowing outflowing material.

subrelativistic velocities ~23,000–34,000 km s 1) and to span low to moderate ionization log U from ~ 2 to ~2.6). The equivalent hydrogen column density of all the components also spans a wide range of values log N_H ~ 20–24 cm 2), with one of them being massive enough to possibly enable feedback from this wind onto the host galaxy.

The *XMM Newton* spectra also con rmed the presence of a strong WA in IRAS 17020 4544, for which only a preliminary modeling was included in L15.

In the present work, we focus our analysis on the WA in IRAS 17020 4544. We report results on its physical properties and characterize its variability between 2004 and 2014.

2. X Ray Observations and Data Reduction

XMM Newton observed IRAS 17020 4544 twice in 2004 for a total exposure time of 40 ks August 30th, OBSID: 0206860101; and September 5th, OBSID: 0206860201) and two more times in 2014 for a total exposure time of 160 ks January 23rd, OBSID: 0721220101; and January 25th, OBSID: 0721220301). There are no background flares during the observations. Standard data processing from the Reflection Grating Spectrometer RGS) den Herder et al. 2001) was carried out with the SAS v13.5.0 tool *rgsproc*. In order to maximize the signal-to-noise, RGS spectra of each epoch were combined in one single spectrum by using the SAS tool *rgscombine*. This can be done because the flux variability within the two *XMM Newton* observations of each epoch is negligible, and there are no spectral changes between them $\Gamma < 5$ and Flux = 3 , where Γ is the continuum spectral slope).

The software used to perform the spectral analysis is XSPEC v.12.10.0c Arnaud 1996).

3. Spectral Analysis

The spectral analysis was performed on the unbinned RGS spectra; therefore, the C-statistic Cash 1979) was applied for the spectral ttings. Errors correspond to a 1 level throughout this work. A ΛCDM cosmology is assumed, with $H_0 = 70$ km s 1 Mpc 1, $\Omega_\Lambda = 0.73$, and $\Omega_M = 0.27$.

3.1. 2014 XMM-Newton Data

We start our analysis by considering the merged RGS data, representative of the spectrum in 2014. Based on our thorough previous analysis of IRAS 17020 4544 L15), we consider a complex model consisting of a power-law X-ray continuum modi ed by Galactic absorption Kalberla et al. 2005) of column density $N_H = 2 \times 10^{20}$ cm 2. The numerous narrow absorption lines imprinted by ionized gas to this continuum, were modeled by means of the self-consistent photoionization code PHASE Krongold et al. 2003). Each one of the PHASE components characterizes one layer of ionized gas in terms of a set of parameters: i) the ionization parameter, de ned as the logarithm of $U = Q\,(4\pi n R^2 c)^{-1}$ Netzer 1987, 2008), where Q is the photon rate integrated over the entire Lyman continuum, n is the gas number density, and R is the gas distance from the nuclear source of photons, ii) the equivalent hydrogen column density, iii) the outflow velocity, and iv) the internal microturbulent velocity. The electron temperature in the PHASE model corresponds to the photoionization equilibrium of the gas. To compute the absorption spectrum of IRAS 17020 4544, we used the same spectral energy distribution SED) as in L15. Four PHASE components were required for modeling the WA, and ve more for the UFO L15). The UFO properties are exhaustively studied and characterized in the narrowband 18–23) in our previous work. In the following, the focus is set on modeling the four WAs in the entire 7–35 band of the RGS spectrum. We initially kept all ve UFO components of L15. However, only the three most signi cant ones $\sigma > 3$ in Table 2 of our previous work) are recovered with equal weight in the entire 7–35 band. This is due to the fact that various free parameters of the remaining two UFO components found at lower signi cance in L15 are not sensitive enough to the broadband data. In addition, when considering the entire RGS band, we note that one UFO component of L15 Comp. A) is better tted by two different phases of gas outflowing at the same velocity more detail in Section 3.3).

The ionization, column density, and velocity of the four WAs and the four UFOs are left free. The internal microturbulent velocity of the gas in the UFO components is xed to 50 km s 1, because this parameter is not sensitive to the data when the absorption lines are very narrow. The turbulent velocity of the WA is left free, together with the power-law photon index and normalization.

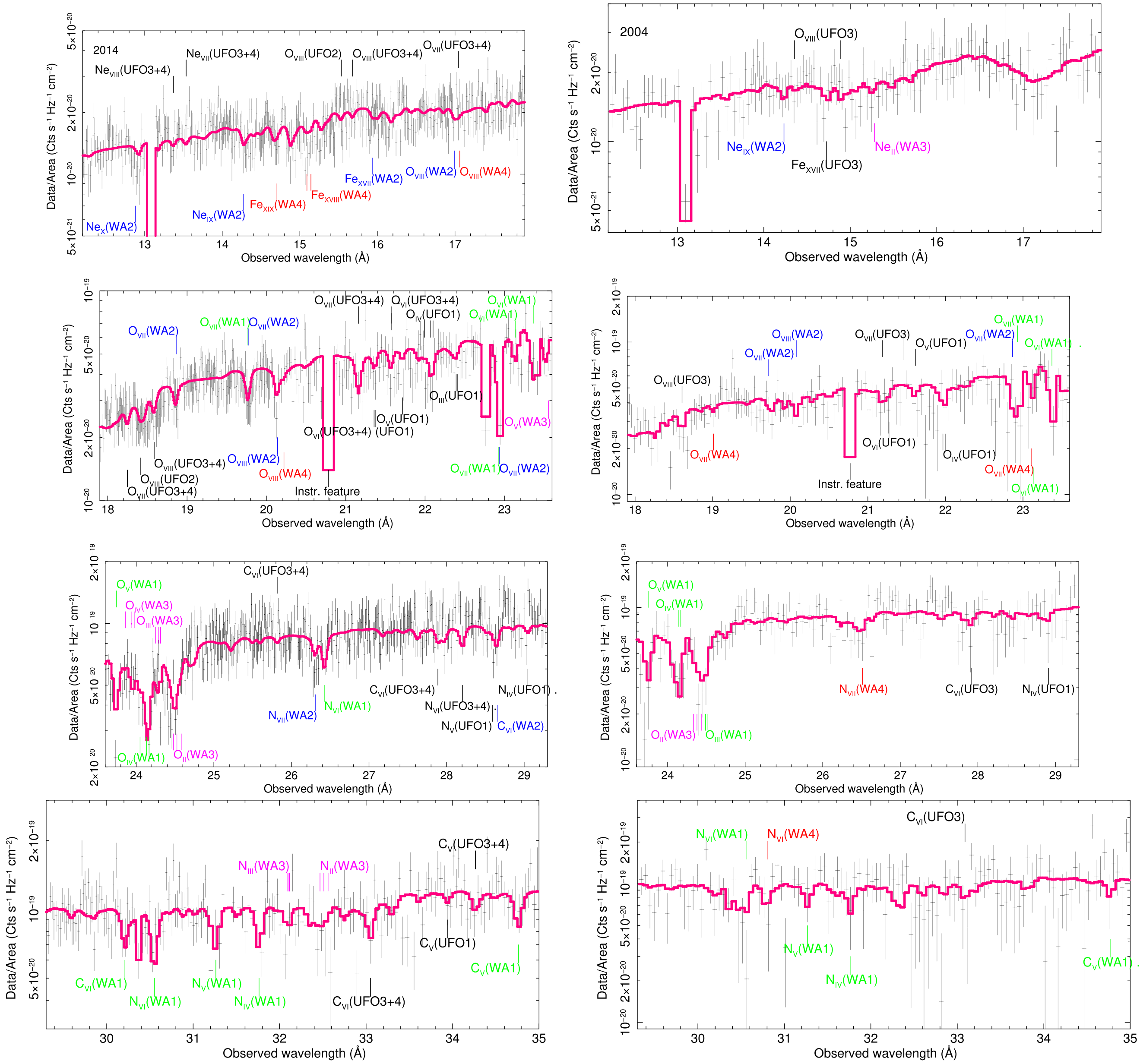

Figure 1. Detector area-corrected data and best- tting model with a Galactic-absorbed continuum 4 WAs 4 2) UFOs applied to the 2014 2004) spectrum on the left-hand right-hand) panels. We show the entire broadband in four wavelength ranges, from top to bottom: 12.2–17.9 , 17.9–23.6 , 23.6–29.3 , and 29.3–35 . The main absorption lines produced by every component are plotted in different colors: WA 1 in green, WA 2 in blue, WA 3 in magenta, WA 4 in red, and the UFOs in black. Every line marked in this gure is included in Table 2.

The best- tting PHASE parameters of the four WAs and four UFOs are shown in the left-hand side of Table 1. We measure a soft flux level of $0.99^{+0.01}_{-0.02} \times 10^{-11}$ erg cm^{-2} s^{-1} tted in the RGS band 7–35 , which is equivalent to the ∼0.3–2 keV range. The power-law photon index is $\Gamma = 2.99^{+0.04}_{-0.01}$, typical of NLS1 galaxies in the soft X-ray band. We nd one of the WAs to be inflowing with a velocity component along the line of sight of 1750 ± 250 km s^{-1}. The most signi cant line associated with this inflow is O VIII at 20.22 , with an equivalent width EW) of ∼9 see component WA 4 in the left-hand panels of Figure 1 and on the left side of Table 2). Two additional components WA 1 and WA 2 in Table 1) are inflowing too at few hundreds of km s^{-1}, although their radial velocities are consistent with 0. That is so because the RGS spectral resolution equals a few hundreds of km s^{-1} at the wavelengths involved den Herder et al. 2001), and the accuracy of the energy scale equals 5 m de Vries et al. 2015). The other WA, which is the least ionized, is instead outflowing at 2300 ± 200 km s^{-1} WA 3, see Table 1, left). The column densities are typical for WAs $N_{\rm H} \sim 10^{20}$–10^{21} cm^{-2}), while the ionization parameters are in the low range log U ∼ 2.5 0.4). The internal microturbulent velocities of the WAs are low, with the largest one being $v_{\rm turb} = 160 \pm 30$ km s^{-1}, which is reflected in narrow, unresolved absorption lines.

Our model provides a robust characterization of the WA and a good description of the data, and yields statistics of $C = 3045$ for 2738 degrees of freedom in the 7–35 band. The inclusion of an additional fth) absorber does not improve the t in a statistical way.

Table 2
Absorption Lines Produced by the Absorbing Components as Identi ed with the PHASE Model in the 2014 and 2004 *XMM Newton* RGS Spectra

Ion	Transition	λ)[a]	Abs.	2014		2004	
				Obs. λ)[b]	EW)	Obs. λ)[b]	EW)
Ne X	$1s^1 \rightarrow 2p^1$ Kα)	12.134	WA 2	12.882 ± 0.001	4 ± 1		
Ne IX	$1s^2 \rightarrow 1s^1 2p^1$ Kα)	13.447	WA 2	14.276 ± 0.001	15 ± 1	14.233 ± 0.001	17^{+1}_{-2}
Ne VIII	$1s^2 2s^1 \rightarrow 1s^1 2s^1 2p^1$ Kα)	13.646	UFO 3	13.369 ± 0.001	8 ± 1		
Ne VIII	”	13.646	UFO 4	13.370 ± 0.001	7 ± 1		
Fe XIX	$2p^4 \rightarrow 2p^3 3d^1$ Lα)	13.795	WA 4	$14.704^{+0.001}_{-0.008}$	2 ± 1		
Ne VII	$2s^2 \rightarrow 1s^1 2s^2 2p^1$ Kα)	13.814	UFO 3	13.534 ± 0.001	13 ± 3		
Ne VII	”	13.814	UFO 4	13.534 ± 0.001	12 ± 3		
Fe XVIII	$2p^5 \rightarrow 2p^4 3d^1$ Lα)	14.158	WA 4	15.092 ± 0.001	2 ± 1		
Fe XVIII	”	14.208	WA 4	$15.144^{+0.001}_{-0.008}$	4 ± 1		
Fe XVIII	”	14.208	WA 4	$15.144^{+0.001}_{-0.008}$	4 ± 1		
Fe XVIII	”	14.256	WA 4	$15.196^{+0.001}_{-0.009}$	2 ± 1		
Ne II	$2p^5 \rightarrow 1s^1 2s^2 2p^6$ Kα)	14.600	WA 3			15.282 ± 0.004	7^{+1}_{-2}
O VIII	$1s^1 \rightarrow 6p^1$	14.634	UFO 3			14.35 ± 0.01	5 ± 3
Fe XVII	$2p^6 \rightarrow 2p^5 3d^1$ Lα)	15.014	UFO 3			14.73 ± 0.01	15 ± 10
Fe XVII	”	15.014	WA 2	15.939 ± 0.001	6^{+3}_{-2}		
O VIII	$1s^1 \rightarrow 4p^1$	15.176	UFO 3			14.89 ± 0.01	8 ± 5
O VIII	$1s^1 \rightarrow 3p^1$ Kβ)	16.006	UFO 2	15.535 ± 0.002	3^{+6}_{-2}		
O VIII	”	16.006	UFO 3	15.681 ± 0.001	7^{+1}_{-3}		
O VIII	”	16.006	UFO 4	15.682 ± 0.001	7 ± 1		
O VIII	”	16.006	WA 2	16.992 ± 0.001	5 ± 1		
O VIII	”	16.006	WA 4	$17.061^{+0.001}_{-0.010}$	3 ± 1		
O VII	$1s^2 \rightarrow 1s^1 5p^1$	17.396	UFO 3	17.043 ± 0.001	8 ± 5		
O VII	”	17.396	UFO 4	17.044 ± 0.001	8 ± 1		
O VII	$1s^2 \rightarrow 1s^1 4p^1$	17.768	WA 2	18.863 ± 0.001	3 ± 1		
O VII	”	17.768	WA 4			19.01 ± 0.02	11 ± 5
O VII	$1s^2 \rightarrow 1s^1 3p^1$ Kβ)	18.627	UFO 3	18.249 ± 0.001	9^{+6}_{-7}		
O VII	”	18.627	UFO 4	18.250 ± 0.001	14 ± 1		
O VII	”	18.627	WA 1	19.769 ± 0.001	32 ± 1		
O VII	”	18.627	WA 2	19.775 ± 0.001	7 ± 1	19.716 ± 0.001	9 ± 1
O VIII	$1s^1 \rightarrow 2p^1$ Kα)	18.969	UFO 2	18.411 ± 0.002	17 ± 5		
O VIII	”	18.969	UFO 3	18.584 ± 0.001	17^{+2}_{-5}	18.61 ± 0.02	20 ± 13
O VIII	”	18.969	UFO 4	18.585 ± 0.001	17 ± 1		
O VIII	”	18.969	WA 2	20.138 ± 0.001	26 ± 1	20.078 ± 0.001	28 ± 2
O VIII	”	18.969	WA 4	$20.220^{+0.001}_{-0.012}$	9 ± 1		
O VII	$1s^2 \rightarrow 1s^1 2p^1$ Kα)	21.601	UFO 3	21.163 ± 0.001	22^{+24}_{-14}	21.19 ± 0.02	18 ± 12
O VII	”	21.601	UFO 4	21.163 ± 0.001	46^{+2}_{-3}		
O VII	”	21.601	WA 1	22.925 ± 0.001	60 ± 2	$22.928^{+0.001}_{-0.007}$	60^{+8}_{-16}
O VII	”	21.601	WA 2	22.932 ± 0.001	32 ± 3	22.864 ± 0.001	37^{+5}_{-7}
O VII	”	21.601	WA 4			23.112 ± 0.001	22 ± 15
O VI	”	21.800	UFO 3	21.358 ± 0.001	7 ± 2		
O VI	”	21.800	UFO 4	21.358 ± 0.001	7^{+2}_{-1}		
O VI	”	21.800	WA 1	23.136 ± 0.001	31 ± 1	$23.140^{+0.001}_{-0.008}$	32^{+2}_{-9}
O VI	$1s^2 2s^1 \rightarrow 1s^1 2s^1 2p^1$ Kα)	22.019	UFO 1	21.371 ± 0.001	9^{+3}_{-5}	21.27 ± 0.01	10 ± 8
O VI	”	22.019	UFO 3	21.573 ± 0.004	20 ± 3		
O VI	”	22.019	UFO 4	21.573 ± 0.001	19^{+3}_{-2}		
O VI	”	22.019	WA 1	23.369 ± 0.001	59 ± 1	$23.372^{+0.001}_{-0.007}$	60^{+6}_{-8}
O V	$2s^2 \rightarrow 1s^1 2s^2 2p^1$ Kα)	22.374	UFO 1	21.716 ± 0.001	16^{+1}_{-3}	21.61 ± 0.01	13 ± 9
O V	”	22.374	WA 1	23.745 ± 0.001	59 ± 1	$23.749^{+0.001}_{-0.008}$	61^{+4}_{-2}
O V	”	22.374	WA 3	23.557 ± 0.004	17 ± 1		
O IV	$2p^1 \rightarrow 1s^1 2s^2 2p^2$ Kα)	22.660	UFO 1	21.993 ± 0.001	8 ± 1		
O IV	”	22.660	WA 1	24.049 ± 0.001	27^{+1}_{-3}		
O IV	”	22.660	WA 3	23.859 ± 0.004	10 ± 1		
O IV	”	22.740	UFO 1	22.071 ± 0.001	17 ± 1	21.97 ± 0.01	12 ± 7
O IV	”	22.740	WA 1	24.134 ± 0.001	47 ± 1	$24.137^{+0.001}_{-0.007}$	51^{+5}_{-2}
O IV	”	22.740	WA 3	23.943 ± 0.004	22 ± 1		
O IV	”	22.770	UFO 1	22.100 ± 0.001	15 ± 1	22.00 ± 0.01	10 ± 7
O IV	”	22.770	WA 1	24.166 ± 0.001	45 ± 1	$24.169^{+0.001}_{-0.008}$	48^{+4}_{-1}
O IV	”	22.770	WA 3	23.974 ± 0.004	18^{+5}_{-1}		
O III	$2p^2 \rightarrow 1s^1 2s^2 2p^3$ Kα)	23.030	WA 3	24.248 ± 0.004	7 ± 1		

Table 2
Continued)

Ion	Transition	λ)[a]	Abs.	2014 Obs. λ)[b]	2014 EW)	2004 Obs. λ)[b]	2004 EW)
O III	”	23.070	UFO 1	22.391 ± 0.001	7^{+3}_{-4}		
O III	”	23.070	WA 1			$24.488^{+0.001}_{-0.008}$	27 ± 7
O III	”	23.070	WA 3	24.290 ± 0.004	8 ± 1		
O III	”	23.090	UFO 1	22.411 ± 0.001	8 ± 4		
O III	”	23.090	WA 1			$24.509^{+0.001}_{-0.008}$	23 ± 7
O III	”	23.090	WA 3	24.311 ± 0.004	14 ± 1		
O II	$2p^3 \rightarrow 1s^1 2s^2 2p^4$ Kα)	23.250	WA 3	24.480 ± 0.004	9 ± 1	$24.332^{+0.004}_{-0.003}$	10 ± 1
O II	$2s^1 2p^4 \rightarrow 1s^1 2s^1 2p^5$ Kα)	23.292	WA 3	24.524 ± 0.004	21 ± 1	24.376 ± 0.003	23^{+6}_{-2}
O II	$2p^3 \rightarrow 1s^1 2s^2 2p^4$ Kα)	23.345	WA 3	24.580 ± 0.004	23 ± 1	$24.431^{+0.004}_{-0.003}$	26^{+5}_{-3}
N VII	$1s^1 \rightarrow 2p^1$ Kα)	24.781	WA 2	26.308 ± 0.001	12 ± 1		
N VII	”	24.781	WA 4			26.56 ± 0.05	7 ± 5
N VI	$1s^2 \rightarrow 1s^1 3p^1$ Kβ)	24.898	WA 1	26.424 ± 0.001	26 ± 1		
C VI	$1s^1 \rightarrow 5p^1$	26.357	UFO 3	25.823 ± 0.001	8^{+1}_{-6}		
C VI	”	26.357	UFO 4	25.823 ± 0.001	7 ± 1		
C VI	$1s^1 \rightarrow 4p^1$	26.990	WA 2	28.653 ± 0.001	4 ± 1		
C VI	$1s^1 \rightarrow 3p^1$ Kβ)	28.466	UFO 3	27.889 ± 0.001	16^{+1}_{-8}	27.92 ± 0.03	8 ± 5
C VI	”	28.466	UFO 4	27.889 ± 0.001	16 ± 1		
C VI	”	28.466	WA 1	30.211 ± 0.001	34^{+2}_{-1}		
N VI	$1s^2 \rightarrow 1s^1 2p^1$ Kα)	28.787	WA 4			30.80 ± 0.02	26 ± 12
N VI	”	28.787	UFO 3	28.203 ± 0.001	24 ± 2		
N VI	”	28.787	UFO 4	28.204 ± 0.001	24^{+1}_{-2}		
N VI	”	28.787	WA 1	30.551 ± 0.001	57^{+2}_{-1}	$30.556^{+0.001}_{-0.010}$	58^{+8}_{-12}
N V	$2s^1 \rightarrow 1s^1 2s^1 2p^1$	29.458	UFO 1	$28.591^{+0.002}_{-0.001}$	6^{+1}_{-3}		
N V	”	29.458	WA 1	31.263 ± 0.001	43 ± 1	$31.268^{+0.001}_{-0.010}$	45^{+1}_{-4}
N IV	$2s^2 \rightarrow 1s^1 2s^2 2p^1$ Kα)	29.928	UFO 1	29.048 ± 0.001	10 ± 1	28.91 ± 0.01	9 ± 5
N IV	”	29.928	WA 1	31.762 ± 0.002	41^{+1}_{-3}	$31.767^{+0.001}_{-0.010}$	42^{+6}_{-1}
N III	$2s^1 2p^2 \rightarrow 1s^1 2s^1 2p^3$ Kα)	30.483	WA 3	32.095 ± 0.005	6 ± 1		
N III	”	30.485	WA 3	32.098 ± 0.006	9 ± 1		
N III	$2p^1 \rightarrow 1s^1 2s^2 2p^2$ Kα)	30.501	WA 3	32.114 ± 0.005	8 ± 1		
N II	$2s^1 2p^3 \rightarrow 1s^1 2s^1 2p^4$ Kα)	30.836	WA 3	32.467 ± 0.006	7 ± 1		
N II	”	30.879	WA 3	32.512 ± 0.005	8 ± 1		
N II	$2p^2 \rightarrow 1s^1 2s^2 2p^3$ Kα)	30.924	WA 3	32.560 ± 0.006	9 ± 1		
C V	$1s^2 \rightarrow 1s^1 5p^1$	32.754	WA 1	34.761 ± 0.001	35 ± 1	$34.767^{+0.001}_{-0.011}$	36^{+2}_{-5}
C VI	$1s^1 \rightarrow 2p^1$ Kα)	33.736	UFO 3	33.053 ± 0.001	32^{+2}_{-24}	33.09 ± 0.03	16 ± 11
C VI	”	33.736	UFO 4	33.053 ± 0.001	34^{+}_{-2}		
C V	$1s^2 \rightarrow 1s^1 3p^1$ Kβ)	34.973	UFO 1	$33.944^{+0.002}_{-0.001}$	12^{+1}_{-3}		
C V	”	34.973	UFO 3	34.264 ± 0.002	18 ± 2		
C V	”	34.973	UFO 4	$34.264^{+0.002}_{-0.001}$	17 ± 2		

Notes. All the atomic transitions data are gathered from the AtomDB database v.3.0.9 Smith et al. 2001), the NIST database v.5.5.6 Kramida et al. 2018), and the XSTAR database v.2.39 Kallman & Bautista 2001). Every absorption line included in this table is depicted in Figure 1.
[a] λ refers to the theoretical wavelength of the absorption line in the source s restframe.
[b] The measured λ values refer to the observer s restframe.

The statistical signi cance of each WA and UFO component is represented by the improvement of ΔC shown in the left side of Table 1. We compute the statistical signi cance of a given absorption component by calculating the improvement in Cash statistics between the best- t with the baseline model, and the best- t obtained when that component is removed from the baseline model.

According to the t parameters reported in the left side of Table 1, the most signi cant components of the wind are WA 1 $\log U \sim$ 1.9, $\log N_{\rm H} \sim 21.1$), and WA 2, with the same column density but higher ionization $\log U \sim$ 0.6), both of which are tracing gas consistent either with being at rest or inflowing at a few hundreds of km s 1. WA 3 is a cooler, fainter component $\log U \sim$ 2.5, $\log N_{\rm H} \sim 20.9$), outflowing at $\sim$2300 km s 1. The fourth and last of the WA components is the most ionized shell $\log U \sim 0.4$), and is inflowing at $\sim 2 \times 10^3$ km s 1.

We now describe the model developed to t the ultra-fast wind in the present work. The UFO here is still structured as a multiphase, multicomponent wind with two different velocities close to $\sim 0.1c$. The rst component is outflowing at 26900 ± 200 km s 1, and is formed by at least two different shells, named UFO 1 and UFO 2 in Table 1. When we leave the velocities of these two shells free to vary independently, we still get the same outflow velocity for both of them. UFO 1 traces a cool and shallow component of the wind $\log U = -2.47^{+0.15}_{-0.19}$, $\log N_{\rm H} = 20.10^{+0.06}_{-0.09}$). On the contrary, UFO 2 is ve orders of magnitude more ionized

($\log U = 2.63^{+0.04}_{-0.13}$) and three orders of magnitude denser ($\log N_H = 23.70 \pm 0.15$).

The second UFO component is formed by two shells as well, named UFO 3 and UFO 4 in Table 1, which are outflowing at 24100 ± 100 km s^{-1}. UFO 3 is a cool, faint layer ($\log U = -0.35^{+0.12}_{-0.19}$, $\log N_H = 20.4^{+0.2}_{-0.4}$), and UFO 4 is cooler and slightly thicker ($\log U \sim -1.22^{+0.10}_{-0.05}$, $\log N_H \sim 20.85^{+0.03}_{-0.06}$).

As in the case of the UFO 1 – UFO 2 component, when the velocities of UFO 3 and UFO 4 are allowed to vary independently, the same outflow velocity is recovered for the two shells. Each component of the flow is therefore identified by its outflow velocity. The need to fit the gas at the same velocity with two separate PHASE components is driven by the very wide range of ionization and column density spanned by the gas, that cannot be fitted by one single PHASE model.

The features imprinted in the 2014 spectrum by the four WAs, as well as by the four UFOs, can be seen in the left panels of Figure 1. Their wavelengths and EWs are gathered on the left side of Table 2.

3.2. 2004 XMM-Newton Data

We consider now the merged RGS spectrum of the two data sets obtained 10 years earlier, in 2004. In our previous work, we inspected the possible presence of a fast wind by applying the best-fit model of 2014 comprising five UFOs. One of these UFO components is confirmed in the 2004 spectrum, and the others cannot be statistically ruled out (see L15 for more detail). Considering the larger spectral band, we recover two of those UFO components, outflowing at $28{,}500 \pm 1000$ km s^{-1} and at $23{,}900 \pm 100$ km s^{-1}, respectively (see the right side of Table 1). Hence, in order to check for variability at long timescales, we apply a model consisting of a locally absorbed power law plus four WAs plus two UFOs to the RGS data from 2004. We compute a flux level of $1.03^{+0.01}_{-0.08} \times 10^{-11}$ erg cm^{-2} s^{-1} in the 0.3–2 keV range, therefore flux variability of the source in a 10 yr lapse is minor. The results of this fit are shown in the right side of Table 1.

WA components nos. 1 and 2 are consistent in 2004 and 2014; thus, it is conceivable that both of them remain at rest (or keep inflowing at few hundreds of km s^{-1}) after a decade. Wind parameters of WA 3 are not consistent in 2004 and 2014; specifically, the large difference in the velocity measured in the two epochs suggests that this WA in 2004 and 2014 most likely originated from two different blobs of gas, both of which are escaping from the system at 4000 ± 200 and 2300 ± 200 km s^{-1}, respectively. As for WA 4, we observe marginal consistency between its column densities in 2004 and 2014, though its ionization in 2014 is between one and two orders of magnitude larger than in 2004; also, this component is still inflowing, but at a lower velocity in 2014 (-1750 ± 250 km s^{-1}, to be compared with -2900 ± 200 km s^{-1} 10 years earlier).

As for the UFOs, we recover the two components at different velocities in the 2004 data, but their multiphase nature cannot be detected (nor can it be statistically ruled out). Both UFO 1 and UFO 3 remain remarkably unvaried within a decade, perhaps indicating the presence of two persistent UFO components (see Table 1).

We interpret the behavior of WA components nos. 3 and 4 in the two observations as the result of the appearance and disappearance of different wind's sections, while WA components nos. 1 and 2 and UFO components 1 and 3 are persistent over a decade (see Section 4). The features imprinted in the 2004 spectrum by the two UFO and the four WA components can be seen in the right-hand panels of Figure 1, and are gathered in the right-hand side of Table 2.

We offer a detailed interpretation of the results from the spectral analysis in Section 4.

3.3. Consistency with Previous Results

In our previous work on the winds system in IRAS 17020+4544, five UFOs were detected and characterized from 2014 *XMM-Newton* data in the 18–23 Å narrowband (see Table 2 in L15). In addition, one of those UFOs was found to be persistent on a 10 yr scale. In this paper, we perform a thorough analysis over the 7–35 Å broadband, recovering three out of the five outflows previously reported. The reason why the two less significant components cannot be constrained in the broadband is because the most prominent spectral features associated with such components are three absorption lines, as reported in Table 1 in L15: O VIII at 18.60 ± 0.03, O III at $21.83^{+0.03}_{-0.01}$, and O IV at $21.55^{+0.03}_{-0.02}$. These lines are significant enough in the 18–23 Å narrowband so that the model parameters of the components producing them in L15 are sensitive to the data in this band. However, in the 7–35 Å broadband their effect gets overwhelmed by the other absorption features. This way, we can neither confirm the presence of the two less significant UFO components, nor rule-out their existence.

The three UFO components that are recovered in this paper are those called "A," "B," and "C" in L15. Component "A" is split here in two phases, namely UFO 3 and UFO 4. Components "B" and "C" are depicted in this work, as in L15, as a single outflow with two phases, UFO 1 and UFO 2, as described in Section 3.1.

As of the 2004 data, two UFO components are recovered. UFO 3, is detected with a significance level of $\Delta C = 36$. This component was already detected in our previous work, where the rest of the UFOs could not be statistically ruled out. In this paper, we find one of those extra components: UFO 1, with a low significance level of $\Delta C = 9$.

4. Discussion

The *XMM-Newton* high-resolution spectra of IRAS 17020+4544 have revealed an outflow characterized by very complex behavior. The source presents the simultaneous presence of a stratified UFO and a multilayered slower absorber whose components are flowing inward and outward. The availability of two spectral epochs allows us to track the evolution of the slower wind along the 10 years elapsed in between the 2 *XMM-Newton* observations. Notably, the UFO does not present any hint of evolution between the two epochs, although this can be said only with respect to the two persistent components that are seen in 2004 and 2014. The following discussion is based on both results from our 2015 paper and from the present work.

4.1. The Source: Properties of IRAS 17020+4544

We first attempt to set some spatial scales and distances for the wind. The launch radii of the outflow component in 2004 and 2014 were estimated by assuming that the outflow velocity must be larger than (or equal to) the escape velocity at the launch radius, which is computed as $R = \frac{2GM_{BH}}{v_{esc}^2}$ by definition.

Considering the outflow velocities measured for WA 3, which is the only WA component outflowing in both epochs, the launch radius must be greater than 8.4×10^{15} cm in 2004 and than 2.5×10^{16} cm 10 years later, in 2014.

Following Elitzur & Shlosman (2006), we compute the dust sublimation radius in this object as $R_{\rm dust} = 0.4 L_{45}^{0.5}$ pc, where L_{45} is the bolometric luminosity of the source in units of 10^{45} erg s^{-1}. Hence, $R_{\rm dust} = 0.3$ pc $= 9 \times 10^{17}$ cm, i.e., the dust sublimation radius is roughly two orders of magnitude larger than the launch radius of the outflow component; therefore, it is likely for the outflow material to be dust-free. With this in mind, together with the results exposed in Sections 3.1 and 3.2, in the following, we investigate three possible interpretations of the nature of the absorbing material detected in IRAS 17020+4544, as well as to its dynamics.

4.2. Shocked Outflow Interpretation

The detection of several components of gas flowing inward and outward at different velocities with the variability pattern observed during the two *XMM-Newton* visits, suggests a different nature of this wind compared to "standard" WAs. Indeed, it is difficult to imagine that such a composite flow of ionized gas resides in external regions like the NLR of the AGN.

The coincidence of the UFO with slower winds moving in opposite directions may be explained in terms of a "shocked outflow." This model predicts that an initial fast outflow radiatively launched at accretion disk scale with outflow velocity $v_{\rm out} \geqslant 10^4$ km s^{-1} shocks with the ambient medium (King 2010; Faucher-Giguère & Quataert 2012; Zubovas & King 2012; King & Pounds 2015). This impact produces first a reverse shock of the wind with the gas located at a radius where the escape velocity is lower than the outflow velocity; therefore, the wind keeps sweeping up the surrounding material and develops a second forward shock. The two shock fronts are separated by a contact discontinuity and whereas the shocked ambient gas could decelerate to velocity of the order of 100 km s^{-1}, the wind shock (reverse) maintains its high velocity while entraining the ambient gas and pushing it further out (Faucher-Giguère & Quataert 2012). In the case of the Narrow Line Seyfert Galaxy NGC 4051, Pounds & Vaughan (2011) also interpreted the signatures of the in–outflowing absorber in that system as the result of a shocked outflow, despite the nondetection of a nuclear ultra-fast wind.

4.3. Instabilities in a Shocked Outflow?

As shown with much higher detail for the case of supernova remnants (SNRs; Velazquez et al. 1998), at the discontinuity between the two shock fronts it is very likely that fluid instabilities (e.g., Rayleigh–Taylor) start developing, since the densities of the impacting wind and of the impacted medium are considerably different. A condition for the Rayleigh–Taylor instability to grow is that the mass of the interstellar medium (ISM) that is pushed by the discontinuity is higher than the mass of the ejecta (Velazquez et al. 1998), which undergoes a deceleration process that is able to trigger instabilities in the fluid. Such instabilities would easily alter the dynamics of the shocked outflow at the scale of the reverse shock and of the discontinuity, and they may give rise to slower components of the wind. It is conceivable that these blobs of gas at different conditions (velocity, ionization, density, and temperature) would be continuously replenished by the effect of the instability and turbulence, and that they may also fall backward instead of following the bulk of the outflow. This behavior is reproduced in simulations of a shocked outflow, where instabilities form turbulent plumes in the front side of the shocked material that reach velocities consistent with those measured in the UFO multicomponents (Longinotti 2018, and A. L. Longinotti et al. in preparation). Depending on which plumes cross our line of sight, absorption lines corresponding to a wide range of velocity components will imprint an emerging absorption spectrum consisting of the combination of several gas components in outflow/inflow plus a stationary wind. Thus, the scenario that we are witnessing in the X-ray spectra of IRAS 17020+4544 seems very consistent with the hypothesis of the shocked outflow described above. In fact, we note that given the spectral resolution of the RGS detectors, the slow inflow velocity measured for WA components nos. 1 and 2 may actually indicate that these shells are stationary. The ionization state and velocity of these gas layers have not changed significantly along the 10 yr timescale explored by *XMM-Newton*. With all probability these components represent the shock itself, whose velocity and likely position have not changed significantly in the 10 years elapsed between the observations.

In this case, the shock cannot overcome gravity and the outflow is in its momentum-conserving phase (see, e.g., King & Pounds 2015). On top of these stationary WAs, we observed significant changes in the velocity of the other two WA components: the apparent deceleration of $\sim$1000 km s^{-1} measured in components nos. 3 and 4 between 2004 and 2014. It is likely that we are seeing different sections of gas rather than the same component changing its velocity. Remarkably, these two components did change their ionization states from 2004 to 2014 (especially WA component no. 4), and since no change of the ionizing continuum is observed (the central source seems completely persistent within the two epochs), we need to invoke other mechanisms to explain the variety of ionization states present in the flowing gas. A viable explanation for this behavior is to postulate that these short-lived blobs (sections of slow gas) are produced in a turbulent regime upon a shocked outflow. The effect of the Rayleigh–Taylor instability due to the different densities of the pre- and post-shock gas is responsible for driving them in and out of our line of sight.

In addition, we also note that shocked outflow models predict that synchrotron radiation is emitted in the core of radio-quiet AGNs due to shock processes (Zakamska & Greene 2014; Nims et al. 2015). Recent results from very long baseline interferometry (VLBI) observations of IRAS 17020+4544 reported by Giroletti et al. (2017), although not conclusively, show that the compact synchrotron emission detected in this source may indicate an origin in a shocked outflow. New deep VLBI observations recently obtained will allow us to gain insights on the association of the radio emission to a shocked outflow (M. Giroletti et al. 2018, in preparation).

4.4. Alternative Interpretations

Other interpretations of the observed outflow pattern are possible, and we explore them in this section. The main observational result that shall be addressed is a valid mechanism of producing different sections/blobs of gas at different ionization states without variations in their ionization being produced by the steady central photoionization source. We are therefore inclined to consider scenarios where clouds or clumps of gas are involved, as it would be difficult to explain the change in ionization and velocity observed over the 10 yr lapse for a continuous distribution of gas.

Elvis 2017) proposes that the warm, radiation pressure driven wind from the accretion disk in AGNs and quasars is the material from which the dense, cool clouds in the BLR are formed, by means of condensation before the WA outflows can reach the escape velocity of the system. Those condensed clouds, unlike the WA, cannot gain acceleration enough to reach the escape velocity. Therefore, they "rain" toward the SMBH as an inflow of short-lived clouds. With respect to our results, these raining clouds could be two different stages of what we called WA components nos. 3 and 4, while nos. 1 and 2 would be the stable, extended, and less dense components from which the others are condensed.

Another possible interpretation is provided by the condensed clouds scenario, which involves no shock. Instead, the inflow occurs via chaotic cold accretion: cold clouds "rain" from the material that cools as it flows away from the launching region see, e.g., Gaspari & Sádowski 2017). Components that do not reach the escape velocity for this system simply fall down again.

However, the condensed clouds scenario cannot explain the ionization of some of the components in this system. In fact, we do not detect cold gas at all, but warm instead $T > 10^4$ K). Finally, considering that freefall velocities computed for this system down to the distances where the WAs are located are roughly ~ 400 km s ^{1}, we conclude that neither of the two alternative scenarios can explain inflow velocities of the order of $(2–3) \times 10^3$ km s ^{1} like the ones detected in the *XMM Newton* spectra.

Therefore, both alternative interpretations fail to provide a consistent explanation of the whole ensemble of observational results derived from IRAS 17020 4544 spectra, leaving the shocked outflow model framework as the most likely scenario for this peculiar wind system.

This paper is based on observations obtained with *XMM Newton*, an ESA science mission with instruments and contributions directly funded by ESA Member States and NASA. The authors wish to thank the anonymous referee for a exhaustive review and useful comments that helped to improve the text. We acknowledge Dr. Pablo Velázquez for his valuable contribution in Section 4.3. M.S. thanks UNAM for support through the DGAPA Program for Post-Doctoral Scholarships. Y.K. acknowledges support from the grant PAIIPIT IN106518. A.L.L. and Y. K. acknowledge nancial support from the ESAC Faculty.

ORCID iDs

Mario Sanfrutos https: orcid.org 0000-0002-2616-544X
Francesca Panessa https: orcid.org 0000-0003-0543-3617

References

Arnaud, K. A. 1996, in ASP Conf. Ser. 101, Astronomical Data Analysis Software and Systems V, ed. G. H. Jacoby & J. Barnes San Francisco, CA: ASP), 17
Blustin, A. J., Branduardi-Raymont, G., Behar, E., et al. 2003, A&A, 403, 481
Blustin, A. J., Page, M. J., Fuerst, S. V., Branduardi-Raymont, G., & Ashton, C. E. 2005, A&A, 431, 111
Cash, W. 1979, ApJ, 228, 939
de Grijp, M. H. K., Keel, W. C., Miley, G. K., Goudfrooij, P., & Lub, J. 1992, A&AS, 96, 389
den Herder, J. W., Brinkman, A. C., Kahn, S. M., et al. 2001, A&A, 365, L7
de Vries, C. P., den Herder, J. W., Gabriel, C., et al. 2015, A&A, 573, A128
Elitzur, M., & Shlosman, I. 2006, ApJL, 648, L101
Elvis, M. 2017, ApJ, 847, 56
Faucher-Giguère, C.-A., & Quataert, E. 2012, MNRAS, 425, 605
Feruglio, C., Fiore, F., Carniani, S., et al. 2015, A&A, 583, A99
Gaspari, M., & Sadowski, A. 2017, ApJ, 837, 149
George, I. M., Turner, T. J., Netzer, H., et al. 1998, ApJS, 114, 73
Giroletti, M., Panessa, F., Longinotti, A. L., et al. 2017, A&A, 600, A87
Gofford, J., Reeves, J. N., Tombesi, F., et al. 2013, MNRAS, 430, 60
Halpern, J. P. 1984, ApJ, 281, 90
Kaastra, J. S., Detmers, R. G., Mehdipour, M., et al. 2012, A&A, 539, A117
Kaastra, J. S., Kriss, G. A., Cappi, M., et al. 2014, Sci, 345, 64
Kaastra, J. S., Mewe, R., Liedahl, D. A., Komossa, S., & Brinkman, A. C. 2000, A&A, 354, L83
Kalberla, P. M. W., Burton, W. B., Hartmann, D., et al. 2005, A&A, 440, 775
Kallman, T., & Bautista, M. 2001, ApJS, 133, 221
Kaspi, S., Brandt, W. N., George, I. M., et al. 2002, ApJ, 574, 643
Kaspi, S., Brandt, W. N., Netzer, H., et al. 2000, ApJL, 535, L17
King, A., & Pounds, K. 2015, ARA&A, 53, 115
King, A. R. 2010, MNRAS, 402, 1516
Komossa, S., & Bade, N. 1998, A&A, 331, L49
Kramida, A., Ralchenko, Y., Reader, J. & NIST ASD Team 2018, NIST Atomic Spectra Database v.5.5.6) Gaithersburg, MD: National Institute of Standards and Technology), https: physics.nist.gov asd
Krolik, J. H., & Kriss, G. A. 2001, ApJ, 561, 684
Krongold, Y., Nicastro, F., Brickhouse, N. S., et al. 2003, ApJ, 597, 832
Krongold, Y., Nicastro, F., Brickhouse, N. S., Elvis, M., & Mathur, S. 2005a, ApJ, 622, 842
Krongold, Y., Nicastro, F., Elvis, M., et al. 2005b, ApJ, 620, 165
Krongold, Y., Nicastro, F., Elvis, M., et al. 2007, ApJ, 659, 1022
Laha, S., Guainazzi, M., Chakravorty, S., Dewangan, G. C., & Kembhavi, A. K. 2016, MNRAS, 457, 3896
Laha, S., Guainazzi, M., Dewangan, G. C., Chakravorty, S., & Kembhavi, A. K. 2014, MNRAS, 441, 2613
Leighly, K. M., Kay, L. E., Wills, B. J., Wills, D., & Grupe, D. 1997, ApJ, 489, L137
Longinotti, A. L. 2018, arXiv:1808.01043
Longinotti, A. L., Krongold, Y., Guainazzi, M., et al. 2015, ApJ, 813, 39
Longinotti, A. L., Krongold, Y., Kriss, G. A., et al. 2013, ApJ, 766, 104
Marconi, A., Risaliti, G., Gilli, R., et al. 2004, MNRAS, 351, 169
Miniutti, G., Sanfrutos, M., Beuchert, T., et al. 2014, MNRAS, 437, 1776
Moran, E. C., Halpern, J. P., & Helfand, D. J. 1996, ApJS, 106, 341
Netzer, H. 1987, MNRAS, 225, 55
Netzer, H. 2008, NewAR, 52, 257
Nims, J., Quataert, E., & Faucher-Giguère, C.-A. 2015, MNRAS, 447, 3612
Pounds, K. A., & Vaughan, S. 2011, MNRAS, 413, 1251
Reynolds, C. S. 1997, MNRAS, 286, 513
Sanfrutos, M., Miniutti, G., Krongold, Y., Agís-González, B., & Longinotti, A. L. 2016, MNRAS, 457, 510
Smith, R. K., Brickhouse, N. S., Liedahl, D. A., & Raymond, J. C. 2001, ApJL, 556, L91
Tombesi, F., Cappi, M., Reeves, J. N., et al. 2013, MNRAS, 430, 1102
Tombesi, F., Cappi, M., Reeves, J. N., & Braito, V. 2012, MNRAS, 422, L1
Tombesi, F., Meléndez, M., Veilleux, S., et al. 2015, Natur, 519, 436
Velazquez, P. F., Gomez, D. O., Dubner, G. M., de Castro, G. G., & Costa, A. 1998, A&A, 334, 1060
Wang, T., & Lu, Y. 2001, A&A, 377, 52
Wisotzki, L., & Bade, N. 1997, A&A, 320, 395
Zakamska, N. L., & Greene, J. E. 2014, MNRAS, 442, 784
Zubovas, K., & King, A. 2012, ApJL, 745, L34